Fragility of ferromagnetic double exchange interactions and pressure tuning of magnetism in 3*d*-5*d* double perovskite Sr_2FeOsO_6

L. S. I. Veiga,[1,2,3,*] G. Fabbris,[1,4] M. van Veenendaal,[1,5] N. M. Souza-Neto,[2] H. L. Feng,[6,7] K. Yamaura,[6,7] and D. Haskel[1,†]

[1]*Advanced Photon Source, Argonne National Laboratory, Argonne, Illinois 60439, USA*

[2]*Laboratório Nacional de Luz Síncrotron, P.O. Box 6192, 13084-971, Campinas, São Paulo, Brazil*

[3]*Instituto de Física "Gleb Wataghin," Universidade Estadual de Campinas, Campinas, São Paulo 13083-859, Brazil*

[4]*Department of Physics, Washington University, St. Louis, Missouri 63130, USA*

[5]*Department of Physics, Northern Illinois University, De Kalb, Illinois 60115, USA*

[6]*Superconducting Properties Unit, National Institute for Materials Science, 1-1 Namiki, Tsukuba, Ibaraki, 305-0044, Japan*

[7]*Graduate School of Chemical Science and Engineering, Hokkaido University, Sapporo, Hokkaido, 060-0810, Japan*

(Received 4 December 2014; revised manuscript received 22 May 2015; published 19 June 2015)

The ability to tune exchange (magnetic) interactions between 3*d* transition metals in perovskite structures has proven to be a powerful route to discovery of novel properties. Here we demonstrate that the introduction of 3*d*-5*d* exchange pathways in double perovskites enables additional tunability, a result of the large spatial extent of 5*d* wave functions. Using x-ray probes of magnetism and structure at high pressure, we show that compression of Sr_2FeOsO_6 drives an unexpected continuous change in the sign of Fe-Os exchange interactions and a transition from antiferromagnetic to ferrimagnetic order. We analyze the relevant electron-electron interactions, shedding light into fundamental differences with the more thoroughly studied 3*d*-3*d* systems.

DOI: 10.1103/PhysRevB.91.235135 PACS number(s): 75.30.Et, 62.50.−p, 75.10.Dg, 78.20.Ls

I. INTRODUCTION

First-row (3*d*) transition metal oxides with perovskite crystal structure (ABO_3 with A an alkali, alkaline earth, or rare earth ion and B a transition metal ion) continue to provide a rich playground for the realization of novel quantum states, a result of a strong interplay between spin, orbital, charge, and lattice degrees of freedom. Manipulation of electron correlations at interfaces of heterostructures or under application of electric and magnetic fields in multiferroic structures has unraveled a plethora of new phenomena in these strongly correlated 3*d* systems [1–5]. In the search for materials with additional tunability, double perovskites with $A_2BB'O_6$ formula unit (B and B′ are distinct TM ions arranged periodically, doubling the unit cell) have emerged as a new fertile ground for exploration of novel quantum states [6,7]. This is because *d*-orbital occupancy and symmetry, which together with lattice distortions control B-B′ electron hopping integrals and therefore transport and exchange (magnetic) interactions, can be independently tuned at B and B′ sites. Additionally, the ability to combine the rather localized 3*d* electron wave functions at B sites with the more delocalized 5*d* electron wave functions of third-row transition metal ions at B′ sites provides a path to further tunability and potential for new functionalities.

While the mechanisms regulating 3*d*-3*d* exchange interactions in these oxide structures are rather well understood in terms of Goodenough-Kanamori (GK) rules [8–11], the understanding of 3*d*-5*d* interactions is much less developed. For example, on-site Coulomb interactions are significantly reduced at 5*d* sites relative to 3*d* sites, affecting the strength of Hund's coupling and related strength of double-exchange interactions (i.e., delocalized superexchange involving e_g electrons) [12–14]. Furthermore, the disparate crystal electric fields (CEF) at 3*d* and 5*d* sites, together with sizable spin-orbit interactions in 5*d* ions with strong nuclear potential, alter the energy landscape and modify electron hopping. As a result, the validity of GK rules in 3*d*-5*d* systems ought to be addressed. The extended 5*d* orbitals may also require accounting for longer-range exchange pathways beyond first neighbor exchange in order to understand magnetic phenomena. A number of double perovskites of this type have shown remarkable properties including half-metallicity above room temperature in A_2CrWO_6 [15], colossal magnetoresistance in Sr_2FeReO_6 [16], and moderate to large magneto-optical properties in Sr_2CrReO_6 and Sr_2CrOsO_6 [17], a testament to the exciting opportunities inherent in the exploration of these versatile structures.

In this work, we explore the use of external pressure (compressive stress) as a tool to modify lattice structure and 3*d*-5*d* exchange interactions, allowing us to develop a fundamental understanding of the underlying physics in a model system, Sr_2FeOsO_6. Using x-ray spectroscopic and structural probes in a diamond anvil cell, we find a pressure-induced reversal in the sign of Fe-Os exchange interactions along the crystallographic *c* axis of this tetragonal structure, driving a change from an antiferromagnetic (AFM) to a ferrimagnetic (FiM) ground state. The transition is a result of an increase in the difference between cubic crystal fields at Fe and Os sites with pressure, which gradually impairs the ability of e_g electrons to mediate ferromagnetic (FM) double exchange (DE) interactions along the *c* axis. As a result, AFM superexchange (SE) involving t_{2g} electrons becomes the dominant interaction in both in-plane and out-of-plane directions at high pressure. This mechanism is different than that behind the AFM-FiM transition induced by chemical pressure (Ca substitution for Sr) where the weakening of

*Present address: Deutsches Elektronen-Synchrotron DESY, Notkestrasse 85, D-22607 Hamburg, Germany.

†Corresponding author: haskel@aps.anl.gov

DE-FM interactions is driven by an increased Fe-O-Os bond buckling along c axis. That both mechanisms lead to a common ground state is striking evidence for a weakened FM interaction as a result of the delocalized nature of $5d$ wave functions, namely, a small on-site Coulomb interaction and large crystal field at Os sites. The novel pressure-induced transition, unique to the $3d$-$5d$ makeup of this double perovskite structure, transforms a material with no remanent magnetization or coercivity into one with robust coercivity (∼0.5 T) typical of permanent magnets, aided by the presence of spin-orbit interaction at Os sites. The fragility of FM interactions in this $3d$-$5d$ system indicates that modest changes in tensile or compressive strain in engineered epitaxial films could have significant impact on magnetic response providing a path to functional devices.

II. EXPERIMENTAL AND THEORETICAL METHODS

A. X-ray absorption spectroscopy

Polycrystalline Ca_2FeOsO_6 and Sr_2FeOsO_6 samples were prepared by solid-state reaction using high-pressure and high-temperature methods as described in Refs. [18,19]. XMCD measurements at Fe $L_{2,3}$ absorption edges were carried out at ambient pressure and low temperature ($T = 15$ K) at undulator beam line 4-ID-C of the Advanced Photon Source. Experiments were performed in polarization switching mode and any artifact in the XMCD data was removed by consecutive measurements in opposite applied fields ($H = 4$ T). The data were collected using total electron yield (TEY) detection mode.

The ambient and high-pressure XMCD measurements at Os $L_{2,3}$ edges were performed at undulator beam line 4-ID-D of the Advanced Photon Source. Higher x-ray harmonics were rejected with two Pd mirrors at 3 mrad incidence angle (critical energy ∼22 keV) and by detuning the second crystal of a Si(111) monochromator to about 80% of the fundamental's intensity. The measurements were done on powder samples in transmission geometry using a helicity modulation technique (13.3 Hz). An external magnetic field of $H = 4$ T was used; measurements were repeated for opposite field directions to remove any artifacts. For XANES and XMCD experiments at high pressure the x-ray beam was focused to 18×22 μm^2 with Kirkpatrick-Baez mirrors. The DAC was prepared with a partially perforated anvil (150 microns wall thickness) opposite a minianvil (0.8 mm in height) on top of a fully perforated anvil to minimize x-ray absorption in the diamond anvils. Culet size was 300 microns. The DAC mounts on a variable-temperature insert of a superconducting magnet for low-temperature measurements down to 1.6 K in applied magnetic fields up to 6.5 T. Powders of Sr_2FeOsO_6 were loaded into a 120 μm hole in a rhenium gasket preindented to 30 μm, together with ruby spheres for *in situ* pressure calibration and neon gas as pressure-transmitting medium.

B. X-ray diffraction

High-pressure XRD experiments were performed at HP-CAT beam line 16-BM-D of the Advanced Photon Source using a symmetric DAC with conical seats and diamond culet size of 300 μm. A 120-μm hole in a rhenium gasket preindented to 30 μm was filled with Sr_2FeOsO_6 powders together with Au and ruby spheres for *in situ* pressure calibration and He gas as pressure-transmitting medium. Pressure was applied manually using a gearbox control system. The measurements were carried out at $T = 15$ K with the x-ray energy tuned to 30 keV. The two-dimensional (2D) XRD patterns were recorded with a MAR345 image plate and converted into 1D plots using the FIT2D software [20]. All the XRD analyses were performed using the LeBail method as implemented in the GSAS/EXPGUI program [21,22].

C. FeO_6 and OsO_6 cluster calculations

The theoretical calculations were done for OsO_6 and FeO_6 clusters with octahedral symmetry. The Hamiltonian includes crystal field, spin-orbit interaction, the full multiplet Coulomb interaction, and the coupling to the nearest-neighbor oxygens. The parameters are calculated within the Hartree-Fock approximation [23] and rescaled to account for band and screening effects. The rescaling for the nonmonopole parts of the Coulomb interaction is 0.45 and 0.8 for Os and Fe, respectively. The on-site Coulomb repulsion between the $5d$/$3d$ electrons is 3 and 6 eV for Os/Fe. The monopole part of the pd Coulomb interaction is 5 and 6 eV for Os and Fe, respectively. The charge-transfer energies are 3 and 0.4 eV, for Os and Fe, respectively. For Os, the spin-orbit interaction strength at ambient pressure is 0.45 eV. At higher pressure, the effective spin-orbit interaction strength is reduced to 0.3 eV to account for the increased osmium bandwidth. The cubic crystal field is 3.7 eV. A small exchange field has been applied. Parameters differ slightly between different compounds to fine-tune the agreement with the experimental spectra. The calculations for Fe are typical for high-spin $3d^5$ compounds. The strong covalency has a relatively weak effect on the spectral line shape. The cubic crystal field is 0.7 eV and the spin-orbit strength at ambient pressure is 59 meV.

III. RESULTS

A. Chemical pressure

We start by comparing the structural and electronic properties of Sr_2FeOsO_6 [19,24] to its chemically compressed analog, Ca_2FeOsO_6 [18]. The smaller Ca^{2+} ions drive a transition from a tetragonal ($I4/m$) to a distorted monoclinic ($P2_1/n$) crystal structure [Fig. 1(a)]. In the tetragonal structure, the $B/B'O_6$ octahedra are rotated by ∼13° around the c axis, leading to buckled (∼167°) Fe-O-Os bonds within the ab plane but retaining Fe-O-Os collinearity along the c axis. This collinear bonding displays FM coupling of Fe and Os ions, as expected from GK rules for the coupling between Fe^{3+} ($3d^5$) and Os^{5+} ($5d^3$) ions [25]. Surprisingly, the in-plane Fe-Os coupling is AFM despite the relatively small buckling angle, in apparent contradiction with GK rules which predict AFM coupling at much larger angles [25]. As discussed below, this is a result of weak $3d$-$5d$ FM interactions relative to their $3d$-$3d$ counterparts, driven by the delocalized nature of the $5d$ wave function. The compressed Ca structure adds a second $B/B'O_6$ octahedra rotation around [110] ($a^-a^-b^+$ in Glazer notation), leading to deviations from collinearity in both in-plane and out-of-plane directions and emergence of

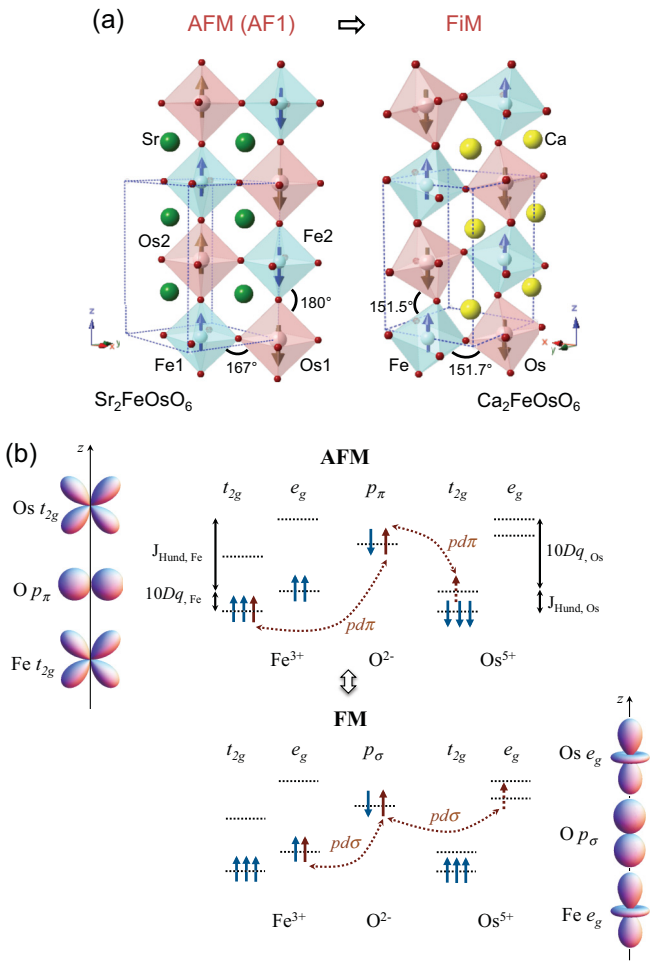

FIG. 1. (Color online) (a) Crystal and magnetic structure of Sr_2FeOsO_6 and Ca_2FeOsO_6 double perovskites. (b) Schematic of double exchange (FM) and superexchange (AFM) interactions between Fe^{3+} and Os^{5+} ions along c axis.

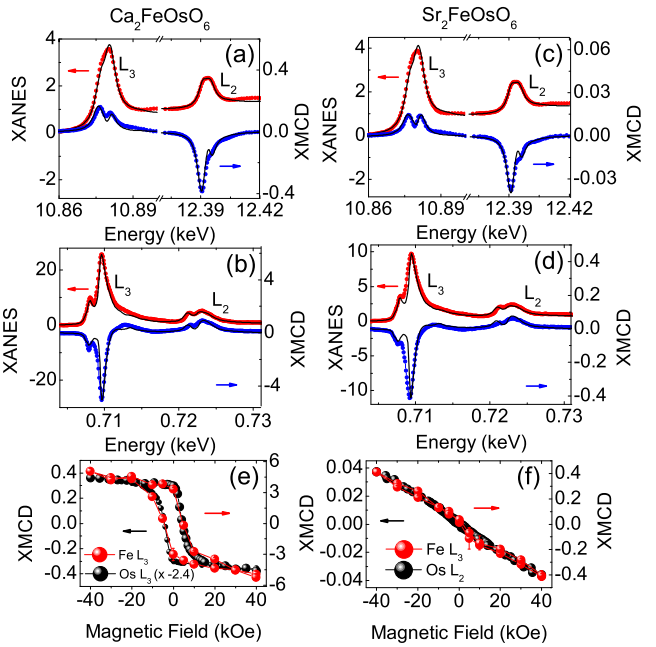

FIG. 2. (Color online) Normalized Os and Fe XANES and XMCD $L_{2,3}$ edge spectra for (a),(b) Ca_2FeOsO_6 and (c),(d) Sr_2FeOsO_6 double perovskites measured at ambient pressure. Black lines are results from cluster calculations. (e),(f) Field dependence of Fe L_3 ($E_{L_3} = 0.709$ keV) and Os $L_{2,3}$ ($E_{L_2} = 12.391$ keV and $E_{L_3} = 10.877$ keV) XMCD peak intensities for Ca_2FeOsO_6 and Sr_2FeOsO_6.

FiM order [Fig. 1(a)]. Note that the FM interaction between Fe and Os is mediated by the overlap of e_g orbitals with oxygen p_σ orbitals, highly sensitive to the degree of Fe-O-Os collinearity [Fig. 1(b), bottom panel]. On the other hand, the AFM interaction is mediated by the overlap of t_{2g} and oxygen p_π orbitals, which is only weakly modified by buckling [see Eq. (1)].

X-ray magnetic circular dichroism (XMCD) measurements at Fe $L_{2,3}$ and Os $L_{2,3}$ edges confirm the presence of FiM order in the Ca structure and absence thereof in the Sr structure (Fig. 2). The Fe and Os magnetic moments point in opposite directions as evidenced by the opposite signs of XMCD signals (Fe along applied field). A strong exchange coupling between magnetic sublattices is evident from their correlated magnetization reversal. The Sr structure shows typical AFM response to applied fields, namely, linear dependence of magnetization due to field-induced canting of Fe and Os moments. The low saturation magnetization in the Sr structure at 4 T, ten times smaller than in the Ca structure [Figs. 2(e) and 2(f)], is indicative of strong exchange interactions favoring a nearly collinear AFM arrangement of magnetic moments with small canting.

Since spin-orbit interactions can affect electronic structure at 5d sites, we performed a theoretical analysis of the x-ray absorption data using OsO_6 and FeO_6 cluster calculations including single and double ligand-hole states. A good agreement between the experimental and theoretical spectra is obtained [see Figs. 2(a)–2(d)]. Calculated orbital and spin moments for Os are $m_l = -\langle L_z \rangle = 0.27\mu_B$/Os and $m_s = -2\langle S_z \rangle = -2.72\mu_B$/Os ($m_{\mathrm{Os}} = m_l + m_s = -2.45\mu_B$/Os). The spin sum rule requires knowledge of $\langle T_z \rangle$, where T_z is the magnetic dipole operator. We used $\langle T_z \rangle = -0.09$. Although small, neglecting this quantity could lead to an underestimation of the spin by more than 20%. The orbital magnetization at Os sites is opposite to the spin magnetization, as expected for a less than half-filled 5d orbital occupancy (calculated number of 5d holes is $n_h = 6.38$). The corresponding quantities for Fe sites are $m_l = 0.044\mu_B$/Fe and $m_s = 4.34\mu_B$/Fe ($m_{\mathrm{Fe}} = 4.38\mu_B$/Fe; number of 3$d$ holes $n_h = 4.35$). The XMCD-derived orbital and spin moments as well as net saturated magnetization ($m_{\mathrm{Fe}} + m_{\mathrm{Os}} = 1.93\mu_B$) are in good agreement with DFT calculations [26] and SQUID measurements [19]. The results confirm a high-spin ground state for Fe, with covalency (and SO interactions at Os sites) responsible for the reduction in moment values from the expected $5(3)\mu_B$ of Fe^{3+}(Os^{5+}) ions in octahedral CEF (neutron diffraction experiments have so far failed to converge on a consistent description of the magnitude of local moments in either structure [27,28]). The orbital-to-spin moment ratio is ten times larger at Os sites due to the stronger SO interaction.

The ground-state expectation value of the angular part of the spin-orbit coupling, $\langle \mathbf{L} \cdot \mathbf{S} \rangle$, can be obtained from the branching ratio (BR) of the isotropic Os absorption spectra $\mathrm{BR} = I_{L_3}/I_{L_2}$, with $I_{L_{2,3}}$ the integrated white line intensities at the $L_{2,3}$ edges, through $\mathrm{BR} = (2+r)/(1-r)$ with $r = \langle \mathbf{L} \cdot \mathbf{S} \rangle / n_h$ and n_h the number of holes in the $5d$ states [29]. We obtain a BR value of 2.6(1) for both compounds, corresponding to $\langle \mathbf{L} \cdot \mathbf{S} \rangle = 0.99\hbar^2$ for the unoccupied $5d$ electron states. Even though the spin-orbit interaction strength, ζ, used in the calculations is comparable to that in the iridates, the spin-orbit coupling in osmates is significantly reduced with respect to these compounds [30–32]. While the SO interaction is still significant, Os cannot be described in the strong spin-orbit coupling limit where three electrons would occupy $j_{\mathrm{eff}} = 3/2$ states [30–32] as this would yield $\langle \mathbf{L} \cdot \mathbf{S} \rangle = 9\zeta/10Dq + 3/2 = 2.66\hbar^2$ using the values from the cluster calculation. A description of Os $5d$ states in terms of pure crystal field (t_{2g}) states is not correct either, as this corresponds to quenched orbital magnetization and a statistical BR = 2. This places the osmates in an intermediate regime where SO interactions compete with Hund's exchange in the presence of a dominant CEF interaction in agreement with calculations [26]. SO and CEF interactions acting on Os $5d$ electrons are expected to be a source of magnetic anisotropy and explain the sizable coercivity of FiM Ca_2FeOsO_6.

B. Compression experiments

We now turn to the effect of hydrostatic pressure on the structural and electronic ground state of Sr_2FeOsO_6. As seen in Figs. 3(c) and 3(d), a continuous increase in XMCD signal is observed under pressure reaching four times its ambient pressure value at 40 GPa (although not matching the saturation value of the Ca structure). The emergence of a FM response in the Os sublattice is clearly seen in the field-dependent XMCD data, where large coercivity (0.5 T) comparable to that of the Ca structure (0.85 T) is observed [Fig. 3(b)]. Remanent magnetization ($\sim 0.23\mu_B$/Os) also emerges. This presents a dramatic change from the negligible coercivity and remanence measured at ambient pressure [Fig. 3(b)]. We note that the XMCD signal fully reverts in size upon pressure reduction from 40 GPa to 24.9 GPa with no measurable hysteresis. It appears that the exchange coupling of Os and Fe moments along the c axis continuously transforms from FM towards AFM under lattice compression leading to a FiM response, mimicking the behavior of the chemically compressed Ca structure [Fig. 1(a)].

One may be tempted to conclude that the driving force for the magnetic transition is a pressure-induced monoclinic distortion with related deviation in Fe-O-Os c-axis bonding from collinearity. However, our low temperature (15 K) x-ray powder diffraction measurements show that the Sr structure remains tetragonal to 56 GPa. The XRD patterns were fitted using LeBail method (EXPGUI-GSAS) within the $I4/m$ tetragonal space group. LeBail refinement yields lattice parameters but does not provide fractional atomic coordinates. Figure 4(a) shows the XRD patterns for Sr_2FeOsO_6 at different

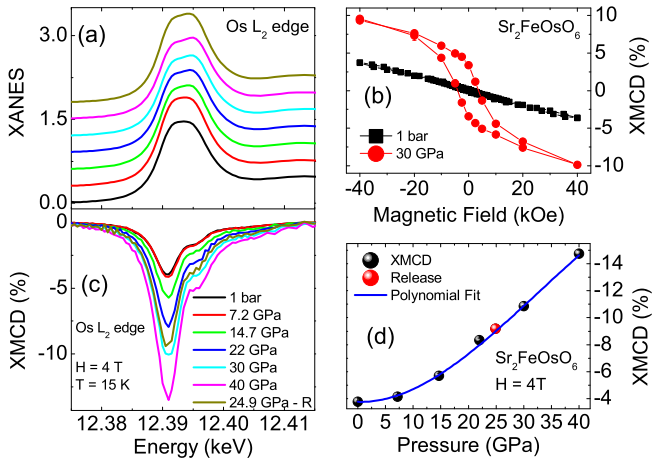

FIG. 3. (Color online) (a) Pressure dependence of Os L_2-edge XANES for Sr_2FeOsO_6. (b) Field dependence of Os L_2-edge XMCD intensity at ambient pressure and at 30 GPa showing emergence of FM response in the Os sublattice. (c),(d) Os L_2-edge XMCD as a function of applied pressure. Data collected after partial pressure release (24.9 GPa) are also shown.

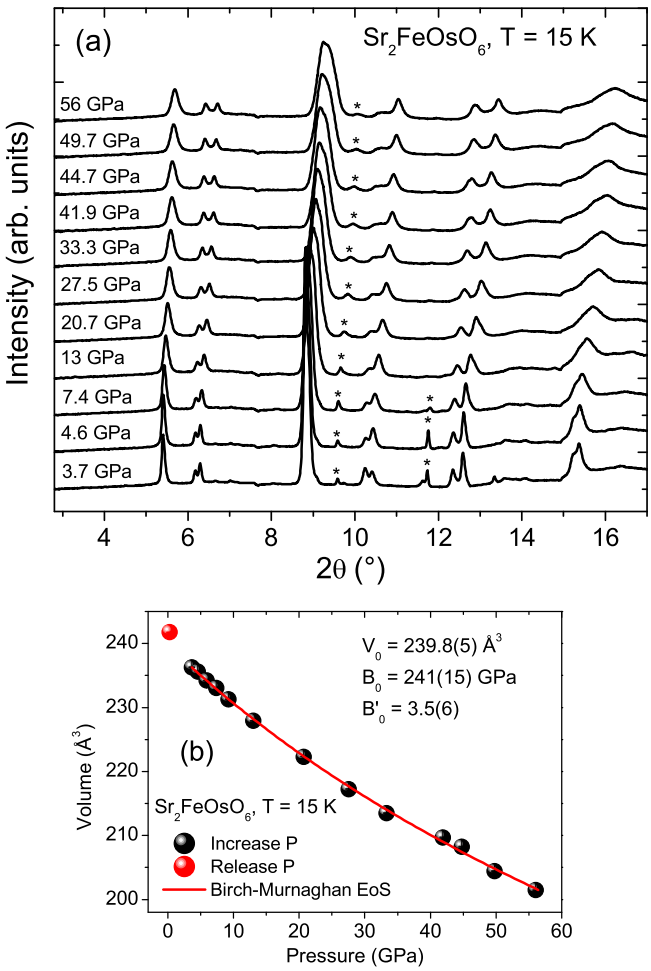

FIG. 4. (Color online) (a) Angle dispersive x-ray powder diffraction of Sr_2FeOsO_6 as a function of pressure at $T = 15$ K. The Bragg peaks marked as * are from Ruby spheres and Au powder. (b) Pressure-volume relationship and its fit to a third-order Birch-Murnaghan equation of state (EOS).

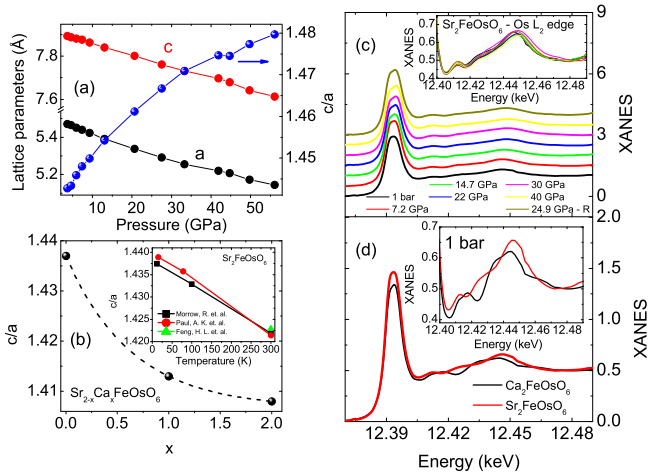

FIG. 5. (Color online) (a) Tetragonal lattice parameters and c/a ratio refined within $I4/m$ tetragonal space group. (b) c/a ratio as a function of Ca doping in $Sr_{2-x}Ca_xFeOsO_6$, and as a function of temperature (ambient pressure) in Sr_2FeOsO_6, reproduced from Refs. [19,24,28]. (c) Pressure dependence of Os L_2-edge XAFS for Sr_2FeOsO_6. (d) Comparison of Os L_2-edge XAFS signal in Ca_2FeOsO_6 and Sr_2FeOsO_6 at ambient pressure.

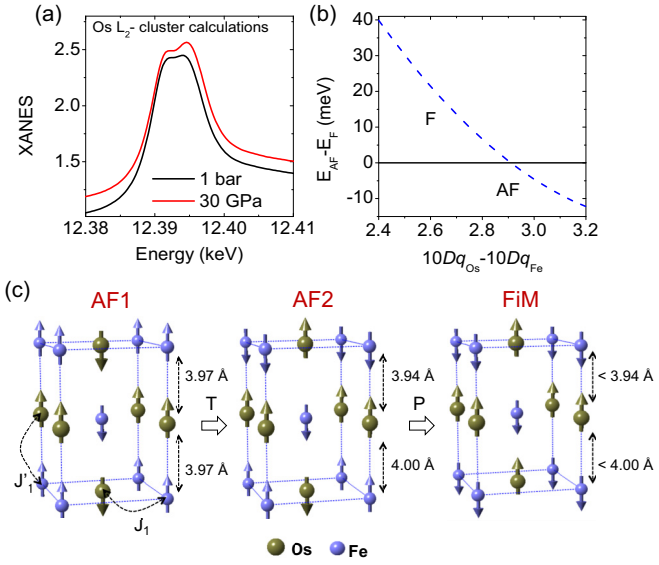

FIG. 6. (Color online) (a) XANES spectra obtained from cluster calculations using octahedral crystal field values of $10Dq = 3.7$ eV and 4.2 eV for ambient pressure and 30 GPa, respectively. (b) Energy difference between FM and AFM Fe-Os coupling along the c axis as a function of the difference in crystal electric field at Os and Fe sites. (c) Evolution of magnetic structure with cooling (T) and applied pressure (P). J_1 (J_1') denotes nearest-neighbor exchange between Fe and Os moments. The Fe-Os distances in AF1 and AF2 structures are taken from Ref. [27]. Note that the magnetic unit cell of the AF2 phase is doubled along the c axis.

pressure points. No discontinuities in lattice parameters or signatures of a structural phase transition were found in the entire pressure range measured. The measured pressure-volume relationship was fitted to a third-order Birch-Murnaghan equation of state, yielding the bulk modulus and its derivative, $B_0 = 241(15)$ GPa, $B_0' = 3.5(6)$, and an ambient pressure volume of $V_0 = 239.8(5)$ Å^3 [Fig. 4(b)].

Ca doping drives a continuous *reduction* in c/a ratio, a result of larger buckling in c-axis Fe-O-Os bonding compressing the c-axis lattice parameter faster than the a-axis lattice parameter [Fig. 5(b)]. This contrasts with the *increase* in c/a ratio with pressure [Fig. 5(a)], which indicates that such c-axis buckling does not take place in the Sr structure. Indeed, an inspection of the tetragonal lattice parameters as a function of pressure indicates that the a-axis contraction rate is almost twofold that of the c-axis [$\frac{\Delta a/a_0}{\Delta P} = -0.1138(3)\%/\text{GPa}$; $\frac{\Delta c/c_0}{\Delta P} = -0.0679(4)\%/\text{GPa}$], with the c/a ratio minimally enhanced up to the highest pressure measured ($\sim$3%). An enhanced c/a ratio is also observed upon cooling the Sr structure at ambient pressure [inset of Fig. 5(b)], which is known to retain tetragonal symmetry with increased in-plane Fe-O-Os buckling. Forcing a model to our diffraction data where the c axis contracts more than the a axis results in an unphysical c/a ratio of 1.36. Such large reduction in c/a ratio would correspond to a significant change in local structure and manifest sizable changes in the x-ray absorption fine structure (XAFS) data [Fig. 5(d)]. However, our XAFS data at the Os L_2 edge shows no significant change to 40 GPa [Fig. 5(c)]. Since XAFS is highly sensitive to deviations in Os-O-Fe bonding from collinearity we conclude that this bonding remains collinear along the c axis and therefore the transition to a FiM state under pressure has a different origin than that induced by chemical pressure.

IV. DISCUSSION

Experimental and theoretical reports on the nature of exchange interactions in Sr_2FeOsO_6 have addressed the origin of AFM order in this structure at ambient pressure [27,28,33]. In fact, two different AFM configurations [AF1 and AF2, Fig. 6(c)] are observed by neutron diffraction to coexist at low temperature, the AF2 phase appearing on cooling below 67 K and becoming dominant below 55 K (85% at 2 K) [27,28]. The AF1 phase consists of FM Fe-Os chains along the c axis, while half of Fe-Os bonds become AFM coupled in the AF2 phase. The change in magnetic structure on cooling may be associated with a lattice distortion in which short (AFM) and long (FM) Fe-Os distances are created [27].

Our powder XRD experiment at high pressure is not sensitive enough to probe for a possible modulation in Fe-Os distances in the c-axis direction in the AF2 phase as reported in Ref. [27]. High pressure single crystal diffraction experiments will be needed to detect whether this modulation, if present, persists under pressure. In any event, both AF1 and AF2 phases carry no net magnetization and are indistinguishable to the XMCD probe. Assuming that the AF2 phase is the ground state at ambient pressure, the application of pressure is seen to drive a second order, reversible transformation into a ferrimagnetic phase. We next discuss the possible origins for this transition.

Comparing the excitations from Fe^{3+} ions ($3d^5$, $t_{2g}^3 e_g^2$ high-spin configuration) and Os^{5+} ions ($5d^3$, $t_{2g}^3 e_g^0$ configuration) along the z direction (c axis), the energy gain due to superexchange mediated by the t_{2g} electrons can be

approximated by

$$\Delta E_{\mathrm{SE}} \approx -2\frac{\alpha^2(pd\pi)^4}{\Delta^2 U}, \tag{1}$$

where Δ is the charge-transfer energy between osmium and oxygen, U is the charge transfer from the Fe site to the Os site, and $(pd\pi)$ is the Slater-Koster overlap integral between t_{2g} orbitals and the π-bonding oxygen orbitals. α is the ratio of the hopping integrals between a transition-metal and oxygen for Os and Fe, where $(pd\pi)$ is significantly larger between Os-O than Fe-O. The factor 2 comes from the fact we are dealing with two t_{2g} orbitals (yz and zx) that delocalize in the z direction. The delocalization of the e_g orbital ($d_{3z^2-r^2}$ orbitals) gives rise to an effective double exchange between Fe and Os given to lowest order by

$$\Delta E_{\mathrm{DE}} \approx -\frac{\alpha^2[(pd\sigma)\cos\frac{180^\circ-\theta}{2}]^4}{\Delta^2} \times \frac{6J_{\mathrm{Hund,Os}}}{(U+10Dq_{\mathrm{Os}}-10Dq_{\mathrm{Fe}})^2}, \tag{2}$$

where θ is the buckling angle along z direction. The antiferromagnetic charge transfer energy is larger for e_g electrons mainly due to the difference in crystal fields ($10Dq_{\mathrm{Os}} - 10Dq_{\mathrm{Fe}}$) since the e_g double exchange requires an excitation into the empty Os e_g orbitals, which are high in energy. The energy gain for the double exchange comes from the ferromagnetic alignment of the magnetic moments of Fe and Os which facilitate the delocalization of the $3z^2 - r^2$ electrons. The energy gain is given by $6J_{\mathrm{Hund,Os}}$ if we assume a simple Hund's exchange interaction between the spins on Os. Since the $5d$ orbitals have a relatively large spatial extent, the Coulomb exchange on Os is significantly smaller than that on Fe. However, the double exchange benefits strongly from the larger hopping matrix elements of the e_g orbitals compared to the t_{2g} orbitals. In the presence of a buckling of the octahedra, the double exchange is more strongly reduced due to the fact that the oxygen σ-bonding orbitals lie along the c axis, whereas the π-bonding orbitals are perpendicular to it. The buckling is included by the $\cos^4(180^\circ - \theta)/2$ term, where $\theta = 180^\circ$ is the angle in the absence of buckling. Buckling therefore reduces the double exchange along the c axis.

Based on the energetics involved in the DE and SE interactions, there are two direct consequences of the reduction in the Fe-O-Os bond lengths. First, there is an increase in the hopping integrals between the TM ions and the oxygens. These are given by the tight-binding parameters $pd\sigma_{\mathrm{TM-O}}$ and $pd\pi_{\mathrm{TM-O}}$ for the σ-bonding e_g orbitals and π-bonding t_{2g} orbitals, respectively. Both hopping matrix elements have a $r_{\mathrm{TM-O}}^{-3.5}$ dependence on the TM-O distance. Additionally, both the SE and DE interactions have, to leading order, a similar dependence on the hopping integrals. Therefore, changes in the relative strengths of the DE and SE interactions are a higher-order effect. This is confirmed by numerical calculations using Fe-O-Os clusters with parameters consistent with those used to calculate the x-ray absorption spectra, which showed a minimal dependence of the *relative* strengths of the exchange interactions with the hopping integrals. The second quantity affected by the reduction of the TM-O distance is the CEF. Here, the magnetic exchange interactions are affected differently. The DE involves the exchange of an e_g electron between the Fe and the Os ion. To leading order the gain in energy due to the DE is given by the Eq. (2). We see that the DE is directly proportional to the (weak) Hund's rule coupling $J_{\mathrm{Hund,Os}}$ on the osmium ion. A decrease in lattice parameters causes an increase in the difference between the Os and Fe crystal-field parameters $10Dq_{\mathrm{Os}} - 10Dq_{\mathrm{Fe}}$, leading to a further reduction of the double exchange interaction. This has been confirmed by cluster calculations where a transition from a FM to AFM Fe-Os coupling is obtained. The on-site parameters are those used in the calculations of x-ray absorption spectra (Fig. 2). Since the effect of the spin-orbit interaction on the ground state is relatively small, the interaction strength was set to zero to obtain a clear spin transition. The hopping parameter $pd\sigma$ between Os and oxygen is 1.4 eV. The value of $pd\pi$ is $0.45\,pd\sigma$. The hopping parameters for Fe are two times smaller. Figure 6(b) shows the difference between the antiferromagnetic and ferromagnetic states as a function of the difference between the osmium and iron crystal fields. The increase in crystal fields stabilizes the antiferromagnetic state, by reducing the double exchange interaction, as expected from Eq. (2). The difference in energy between the two spin states changes by several tens of meV for a change in crystal field by a few hundreds of meV. Evidence for pressure-induced changes in the CEF parameter at Os sites is seen in the evolution of the L_2-edge white line [Fig. 3(a)], the enhanced spectral weight in the high-energy side reproduced in cluster calculations with a 0.5 eV increase in crystal field strength [Fig. 6(a)].

An understanding of the pressure induced magnetic transition naturally follows. Upon lattice compression the reduction in all Fe-Os distances and related increase in (cubic) CEF energy causes a weakening of an already fragile Fe-Os DE-FM interaction relative to the SE-AFM interaction along the c axis. The in-plane Fe-Os coupling remains AFM at all temperatures and pressures due to the persistent in-plane Fe-O-Os buckling. The transition to AFM coupling in Fe-Os bonds along the c axis leads to emergence of FiM order in the compressed structure. Although full, collinear FiM order is not achieved at 40 GPa (based on field dependent data and comparison to Ca analog), the transition appears to be second order as no detectable hysteresis was observed on pressure release.

The high degree of tunability of exchange interactions under pressure is unique to the $3d$-$5d$ makeup of this double-perovskite structure, namely, the delocalized $5d$ state reduces the on-site Coulomb interaction and increases CEF resulting in weaker DE-FM Fe-Os interactions compared to those found in $3d$-$3d$ analogs. For example, the FM state of La_2MnNiO_6 remains unchanged to at least 38 GPa, a result of strong on-site (Hund's) coupling on Mn sites [34]. The ability to not only dramatically alter the magnetic state with external stimuli but to do so in a continuous fashion is appealing for applications where tunability of coercivity and saturation magnetization is desired. While undoped Sr_2FeOsO_6 requires sizable pressures (>10 GPa) to induce significant changes in coercivity and net magnetization, one can envision doping Ca into the Sr structure to attain proximity to a FiM state [28], hence enabling much smaller pressures (or strain in films) to drive the AFM-FiM transition in a reversible way; e.g., with dynamical compression/decompression. Furthermore, the ability to

achieve sizable coercive fields (0.5 T) by manipulating indirect ($3d$-$5d$) exchange interactions with pressure coupled with SO interactions at $5d$ sites presents an interesting opportunity in the search for rare-earth free permanent magnets [35,36].

ACKNOWLEDGMENTS

Work at Argonne is supported by the US Department of Energy, Office of Science, Office of Basic Energy Sciences, under Contract No. DE-AC02-06CH11357. L.S.I.V. is supported by FAPESP (SP-Brazil) under Contract No. 2013/14338-3. M.v.V. was supported by DOE-BES under Grant No. DE-FG02-03ER46097. This research was supported in part by the World Premier International Research Center of the Ministry of Education, Culture, Sports, Science and Technology (MEXT) of Japan, the Japan Society for the Promotion of Science (JSPS) through a Grant-in-Aid for Scientific Research (25289233). We would like to thank Changyong Park and Curtis Kenney-Benson for their assistance at 16-BM-D beamline, Sergey N. Tkachev for assistance with gas loading, and Richard Rosenberg for help with soft x-ray measurements. We also thank GSECARS for use of the gas loading and laser drilling facilities.

[1] M. Huijben, G. Rijnders, D. H. A. Blank, S. Bals, S. V. Aert, J. Verbeeck, G. V. Tendeloo, A. Brinkman, and H. Hilgenkamp, Nat. Mater. **5**, 556 (2006).
[2] A. Ohtomo, D. A. Muller, J. L. Grazul, and H. Y. Hwang, Nature (London) **419**, 378 (2002).
[3] S.-W. Cheong and M. Mostovoy, Nat. Mater. **6**, 13 (2007).
[4] Y. Tokunaga, N. Furukawa, H. Sakai, Y. Taguchi, T.-h. Arima, and Y. Tokura, Nat. Mater. **8**, 558 (2009).
[5] R. Ramesh and N. A. Spaldin, Nat. Mater. **6**, 21 (2007).
[6] T. Saha-Dasgupta, J. Supercond. Nov. Magn. **26**, 1991 (2013).
[7] V. Pardo and W. E. Pickett, Phys. Rev. B **80**, 054415 (2009).
[8] P. W. Anderson, Phys. Rev. **79**, 350 (1950).
[9] J. B. Goodenough, Phys. Rev. **100**, 564 (1955).
[10] J. B. Goodenough, J. Phys. Chem. Solids **6**, 287 (1958).
[11] J. Kanamori, J. Phys. Chem. Solids **10**, 87 (1959).
[12] C. Zener, Phys. Rev. **82**, 403 (1951).
[13] J. Kanamori and K. Terakura, J. Phys. Soc. Jpn. **70**, 1433 (2001).
[14] P. Anderson and H. Hasegawa, Phys. Rev. **100**, 675 (1955).
[15] J. B. Philipp, P. Majewski, L. Alff, A. Erb, R. Gross, T. Graf, M. S. Brandt, J. Simon, T. Walther, W. Mader *et al.*, Phys. Rev. B **68**, 144431 (2003).
[16] K.-I. Kobayashi, T. Kimura, Y. Tomioka, H. Sawada, K. Terakura, and Y. Tokura, Phys. Rev. B **59**, 11159 (1999).
[17] H. Das, M. De Raychaudhury, and T. Saha-Dasgupta, Appl. Phys. Lett. **92**, 201912 (2008).
[18] H. L. Feng, M. Arai, Y. Matsushita, Y. Tsujimoto, Y. Guo, C. I. Sathish, X. Wang, Y.-H. Yuan, M. Tanaka, and K. Yamaura, J. Am. Chem. Soc. **136**, 3326 (2014).
[19] H. L. Feng, Y. Tsujimoto, Y. Guo, Y. Sun, C. I. Sathish, and K. Yamaura, High Press. Res. **33**, 221 (2013).
[20] A. P. Hammersley, S. O. Svensson, M. Hanfland, A. N. Fitch, and D. Hausermann, High Press. Res. **14**, 235 (1996).
[21] A. C. Larson and R. B. Von Dreele, *General Structure Analysis System (GSAS)* (Los Alamos National Laboratory, Report LAUR, 86-748, 2000).
[22] B. H. Toby, J. Appl. Crystallogr. **34**, 210 (2001).
[23] B. T. Thole, G. van der Laan, J. C. Fuggle, G. A. Sawatzky, R. C. Karnatak, and J.-M. Esteva, Phys. Rev. B **32**, 5107 (1985).
[24] A. K. Paul, M. Jansen, B. Yan, C. Felser, M. Reehuis, and P. M. Abdala, Inorg. Chem. **52**, 6713 (2013).
[25] J. B. Goodenough, *Magnetism and the Chemical Bond* (Interscience, New York, 1963).
[26] H. Wang, S. Zhu, X. Ou, and H. Wu, Phys. Rev. B **90**, 054406 (2014).
[27] A. K. Paul, M. Reehuis, V. Ksenofontov, B. Yan, A. Hoser, D. M. Többens, P. M. Abdala, P. Adler, M. Jansen, and C. Felser, Phys. Rev. Lett. **111**, 167205 (2013).
[28] R. Morrow, J. F. Freeland, and P. Woodward, Inorg. Chem. **53**, 7983 (2014).
[29] G. van der Laan and B. T. Thole, Phys. Rev. Lett. **60**, 1977 (1988).
[30] B. J. Kim, H. Ohsumi, T. Komesu, S. Sakai, T. Morita, H. Takagi, and T. Arima, Science **323**, 1329 (2008).
[31] D. Haskel, G. Fabbris, M. Zhernenkov, P. P. Kong, C. Q. Jin, G. Cao, and M. van Veenendaal, Phys. Rev. Lett. **109**, 027204 (2012).
[32] M. A. Laguna-Marco, D. Haskel, N. Souza-Neto, J. C. Lang, V. V. Krishnamurthy, S. Chikara, G. Cao, and M. van Veenendaal, Phys. Rev. Lett. **105**, 216407 (2010).
[33] S. Kanungo, B. Yan, M. Jansen, and C. Felser, Phys. Rev. B **89**, 214414 (2014).
[34] D. Haskel, G. Fabbris, N. M. Souza-Neto, M. van Veenendaal, G. Shen, A. E. Smith, and M. A. Subramanian, Phys. Rev. B **84**, 100403 (2011).
[35] H. Zeng, J. Li, J. P. Liu, Z. L. Wang, and S. Sun, Nature (London) **420**, 395 (2002).
[36] B. Balamurugan, B. Das, W. Y. Zhang, R. Skomski, and D. J. Sellmyer, J. Phys.: Condens. Matter **26**, 064204 (2014).